Supplementary information

A stable dual-emitting dye@LMOF luminescence probe for rapid and visible detection of organophosphorous pesticides in aqueous medium †

Jie Zhang,[a] Wendi Zhou,[a] Lijun, Zhai,[a] Xiaoyan Niu, [a] and Tuoping Hu*[a]

X-ray crystallography

Diffraction data collections for **1** was finished on a Bruker Smart Apex II CCD area-detector diffractometer with graphite-monochromated Mo Kα radiation (λ = 0.71073 Å). The integration of the diffraction data as well as the intensity corrections for the Lorentz and polarization effects, was carried out using the SAINT program. Semi-empirical absorption correction was performed using SADABS program. The structure of **1** was solved by direct methods and all the non-hydrogen atoms were refined anisotropically on F^2 by the full-matrix least-squares technique with olex. The hydrogen atoms except for those of water molecules were generated geometrically and refined isotropically using the riding model. Because the guest solvent molecules in MOF **1** are highly disordered and impossible to refine using conventional discrete-atom models, the SQUEEZE subroutine of the *PLATON* software suite was used to remove the scattering from the highly disordered solvent molecules. The formula of MOF **1** was obtained based on volume/count electron analysis, TGA and elemental analysis. The reported refinements are of the guest-free structures obtained by the SQUEEZE routine, and the results are attached to the CIF file. The details of the crystal data for **1** are summarized in Table S1, and selected bond lengths and angles are listed in Table S2 (ESI†).

Table S1 Crystal data and structure refinements for LMOF **1.**

MOF	LMOF **1**
Empirical formula	$C_{78}H_{46}Cd_3N_4O_{18}$
Formula weight	1664.39
Crystal system	Triclinic
Space group	*P*-1
a (Å)	11.143(6)
b (Å)	14.102(7)
c (Å)	16.934(9)
α(°)	105.376(8)
β(°)	96.152(9)
γ(°)	105.376(8)
V (Å^3)	2422(2)
Z	1
Dc (g cm^{-3})	1.141
μ(mm^{-1})	0.707
F (000)	830.0
Reflections collected	13452
Independent reflections	9702
Goodness-of-fit	0.887
R_1[a] [$I > 2\sigma(I)$]	0.0477
wR_2[b] [$I > 2\sigma(I)$]	0.1075
CCDC number	1960249

[a]$R_1 = \Sigma||F_o|-|F_c||/\Sigma|F_o|$. [b]$wR_2 = |\Sigma w(|F_o|^2-|F_c|^2)|/\Sigma|w(F_o)^2|^{1/2}$

Table S2 Crystal data and structure refinements for LMOF **1**.

LMOF **1**					
Cd1-O1^1	2.236(4)	Cd1-O6^3	2.292(3)	Cd2-O7^2	2.415(4)
Cd1-O1	2.236(4)	Cd1-O9^4	2.283(4)	Cd2-O10^4	2.186(4)
Cd1-O6^2	2.292(3)	Cd1-O9^5	2.283(4)	Cd2-N1	2.357(6)
Cd2-O6^2	2.339(3)	Cd2-O2	2.211(4)	Cd2-N2	2.340(5)
O1^1-Cd1-O1	180.0	O1-Cd1-O9^4	89.32(14)	O9^5-Cd1-O6^3	95.10(12)
O1-Cd1-O6^2	90.37(13)	O1-Cd1-O9^5	90.68(14)	O9^5-Cd1-O6^2	84.90(12)
O1^1-Cd1-O6^3	90.37(13)	O1^1-Cd1-O9^5	89.32(14)	O9^4-Cd1-O6^3	84.90(12)
O1^1-Cd1-O6^2	89.63(13)	O6^3-Cd1-O6^2	180.0	O9^4-Cd1-O9^5	180.0
O1-Cd1-O6^3	89.63(13)	O9^4-Cd1-O6^2	95.10(12)	O2-Cd2-O6^3	101.36(15)
O1^1-Cd1-O9^4	90.68(14)	N1-Cd2-O7^3	94.99(19)	O2-Cd2-O7^3	155.63(15)
O10^5-Cd2-O2	92.08(16)	N2-Cd2-O7^3	87.09(14)	O2-Cd2-N1	88.0(2)
O10^5-Cd2-O6^3	111.11(15)	N2-Cd2-N1	70.5(2)	O2-Cd2-N2	116.52(16)
O10^5-Cd2-O7^3	94.70(16)	O6^3-Cd2-N2	136.90(13)	O6^3-Cd2-O7^3	54.42(12)
O10^5-Cd2-N1	156.1(2)	O10^5-Cd2-N2	88.30(18)	O6^3-Cd2-N1	92.25(18)

Table S3. LoD and LoQ of RhB@LMOF **1** toward pesticides at room temperature.

Analytes	LoD	LoQ
parathion-methyl	1.2×10^{-5}	3.9×10^{-5}
parathion	0.43×10^{-5}	1.43×10^{-5}
nitenpyram	5.36×10^{-5}	1.78×10^{-6}
thiamethoxam	5.07×10^{-5}	1.69×10^{-6}
carbaryl	5.98×10^{-5}	1.99×10^{-6}
atrinze	1.05×10^{-4}	3.49×10^{-5}

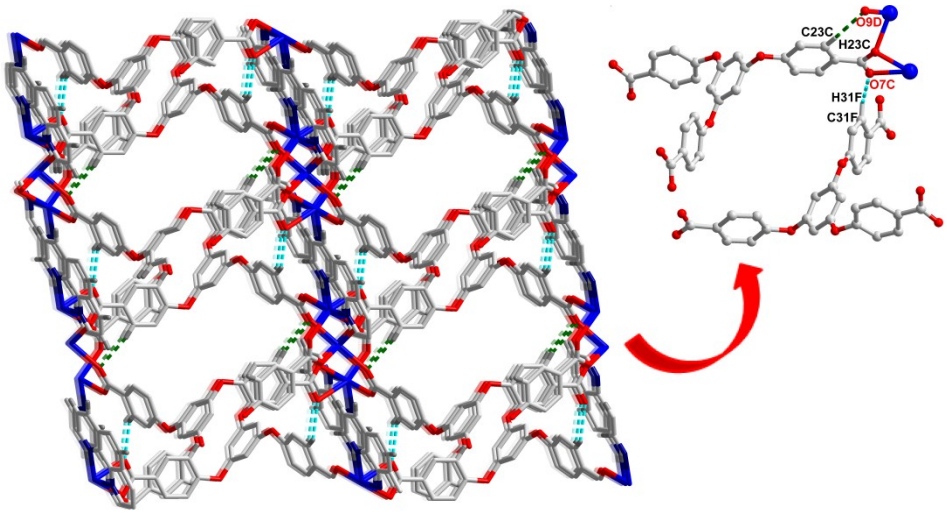

Fig. S1. The hydrogen bonds interaction between the 3D supermolecule structure of LMOF **1**.

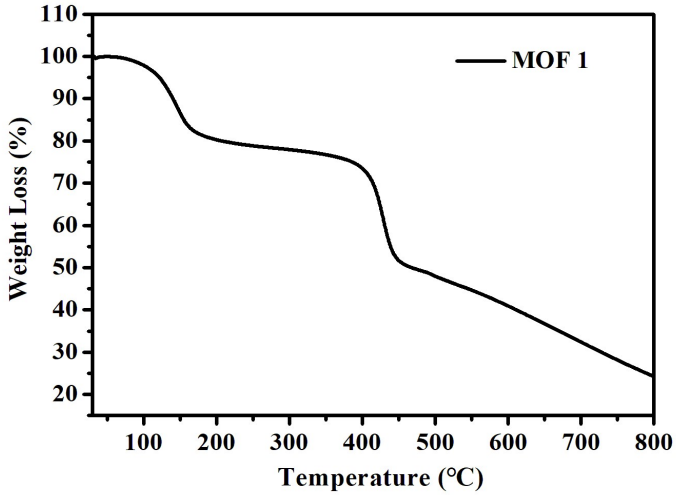

Fig. S2 The TG curve for LMOF **1.**

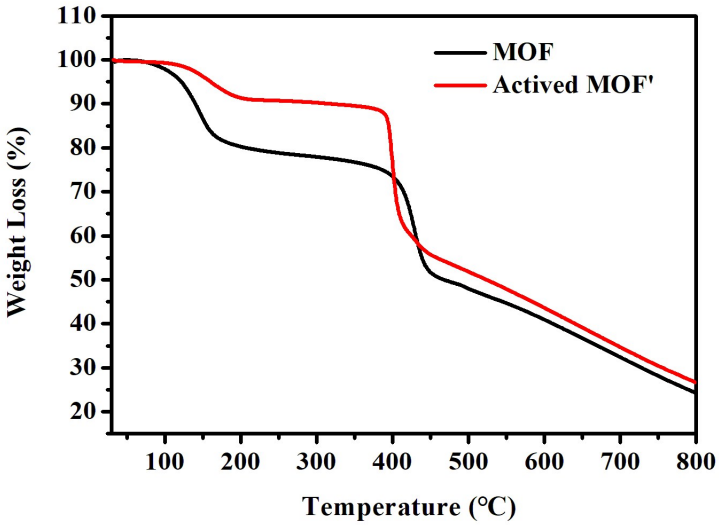

Fig. S3 The TG curve for activted LMOF **1**'.

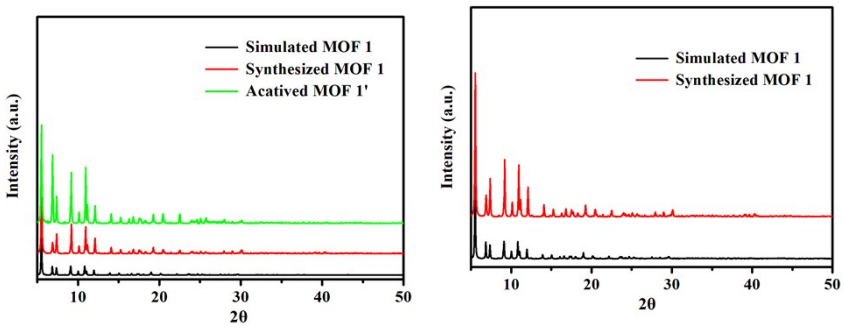

Fig. S4. The PXRD pattern for LMOF **1** and activated LMOF **1**'.

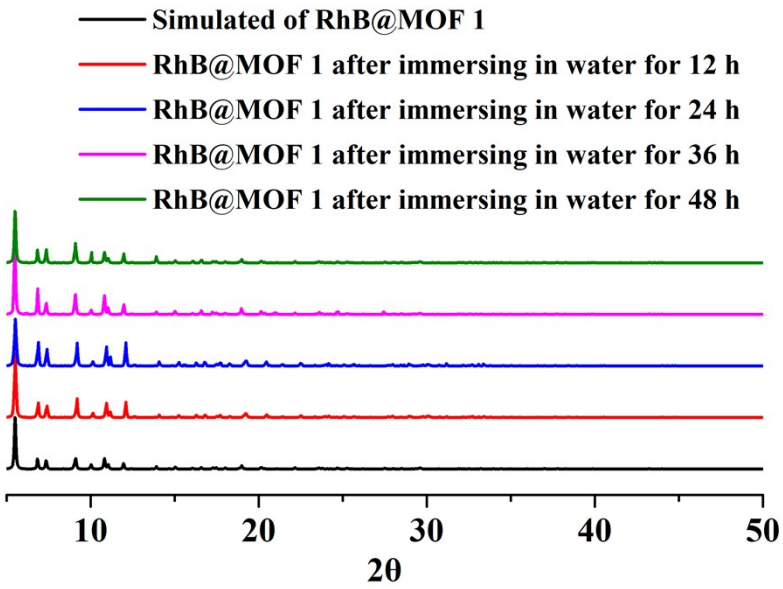

Fig. S5. The PXRD pattern for RhB@LMOF **1** after immersing in water for various times.

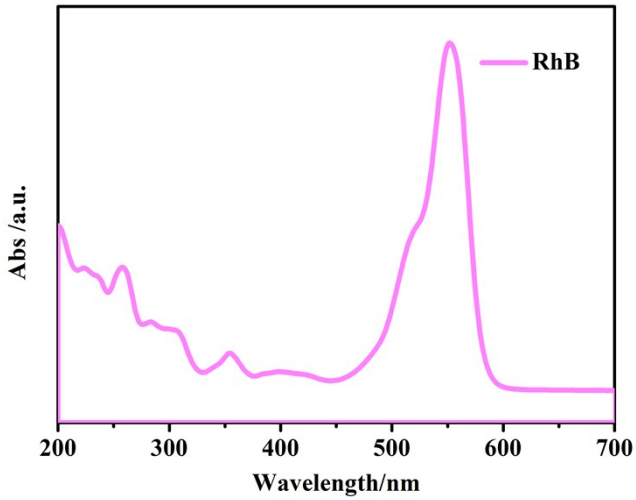

Fig. S6. The absorption spectrum for RhB under the UV-light.

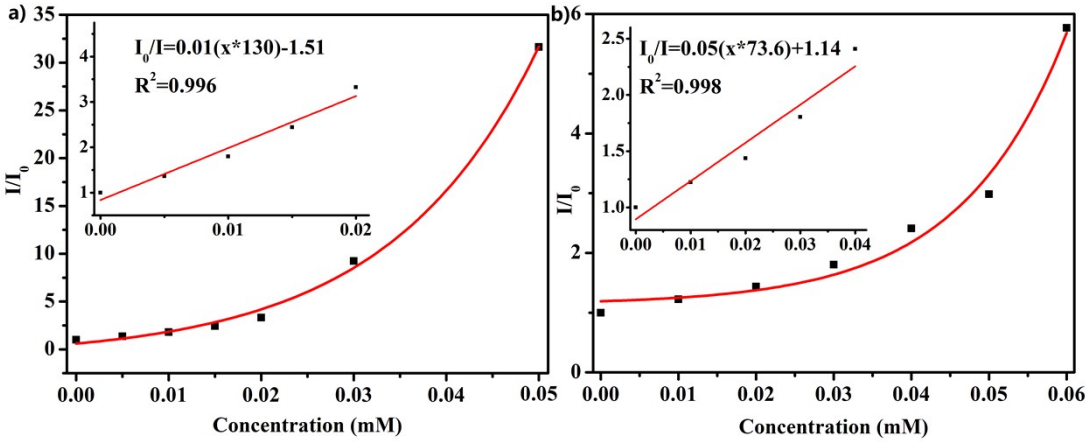

Fig. S7. The Ksv plot for the fluorescence quenching of parathion (a)/parathion-methyl (b)@RhB@LMOF **1** suspensions, inset the Ksv plot at low concentration.

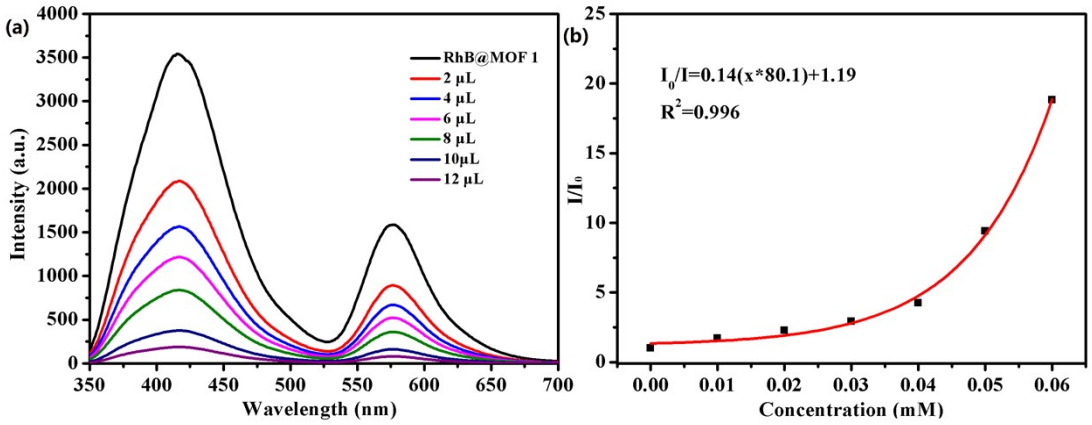

Fig. S8. Emission spectra for RhB@LMOF **1** with the addition of different concentrations of nitenpyram, The Ksv plot for the fluorescence quenching of nitenpyram@RhB@LMOF **1** suspension.

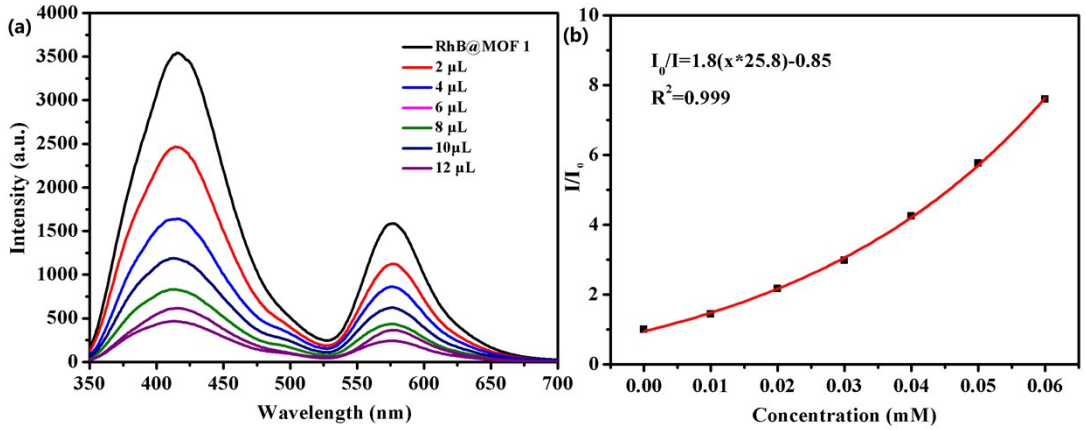

Fig. S9. Emission spectra for RhB@LMOF **1** with the addition of different concentrations of thiamethoxam, The Ksv plot for the fluorescence quenching of thiamethoxam @RhB@LMOF **1** suspension.

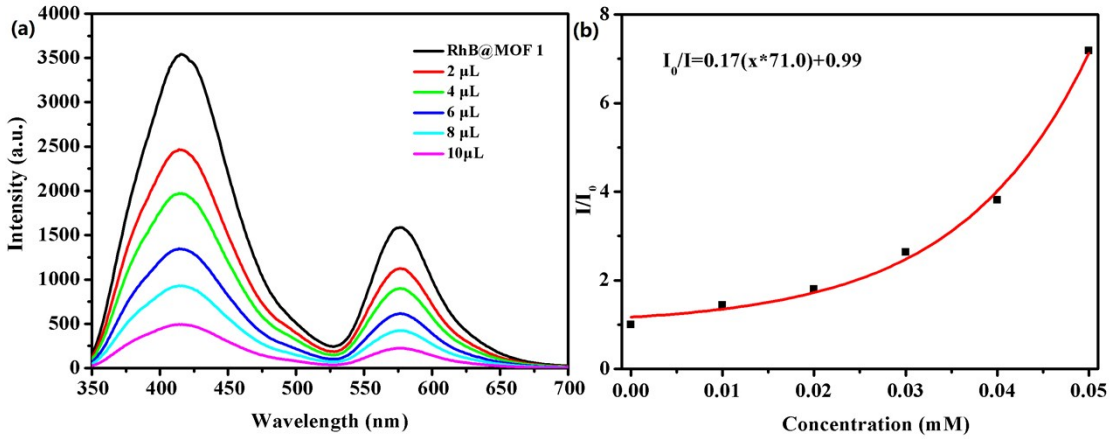

Fig. S10. Emission spectra for RhB@LMOF **1** with the addition of different concentrations of carbaryl, The Ksv plot for the fluorescence quenching of carbaryl@RhB@LMOF **1** suspension.

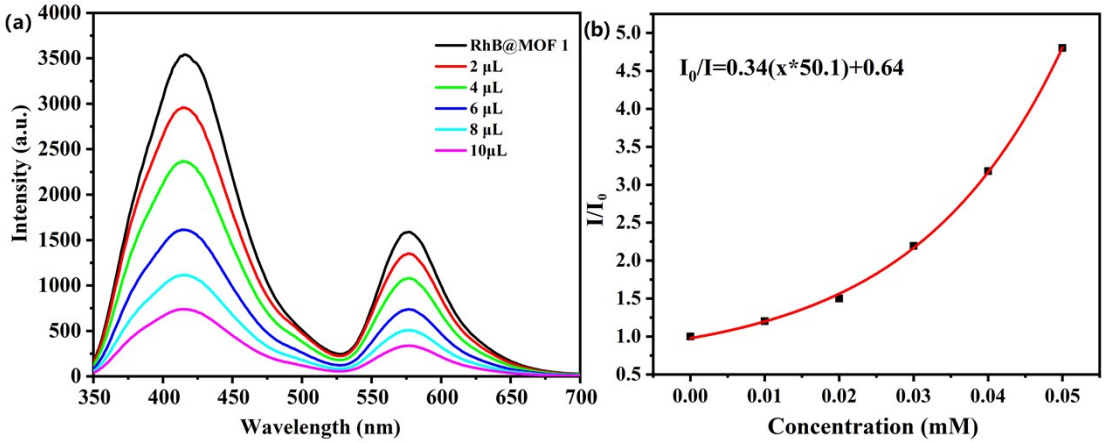

Fig. S11. Emission spectra for RhB@LMOF **1** with the addition of different concentrations of atrinze, The Ksv plot for the fluorescence quenching of atrinze@RhB@LMOF **1** suspension.

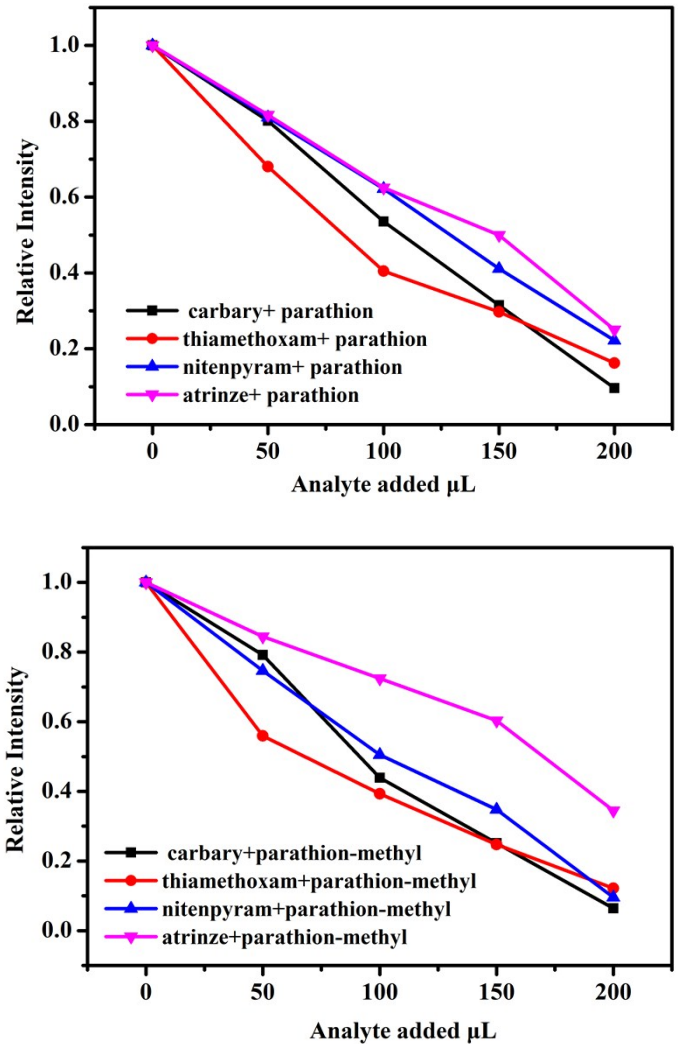

Fig. S12. The selective detection of parathion/parathion-methyl on RhB@LMOF **1** in the presence of carbary/thiamethoxam/nitenpyram/atrinze in water.

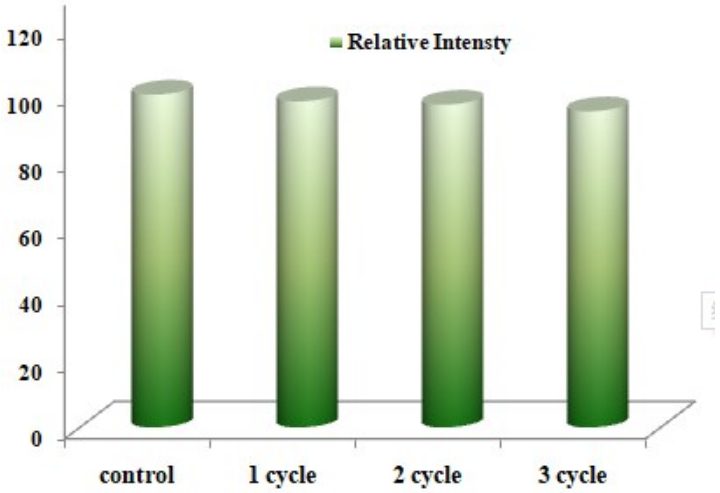

Fig. S13. The relative intensity of **1** after treated with parathion after three cycles.

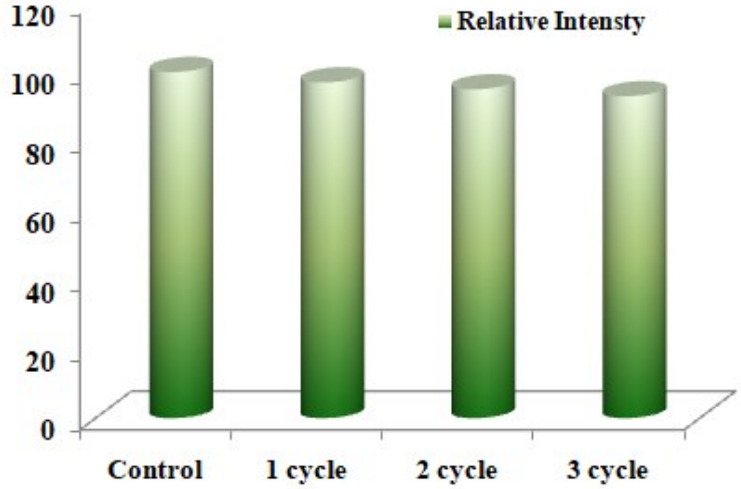

Fig. S14. The relative intensity of RhB@LMOF **1** after treated with parathion-methyl after three cycles.

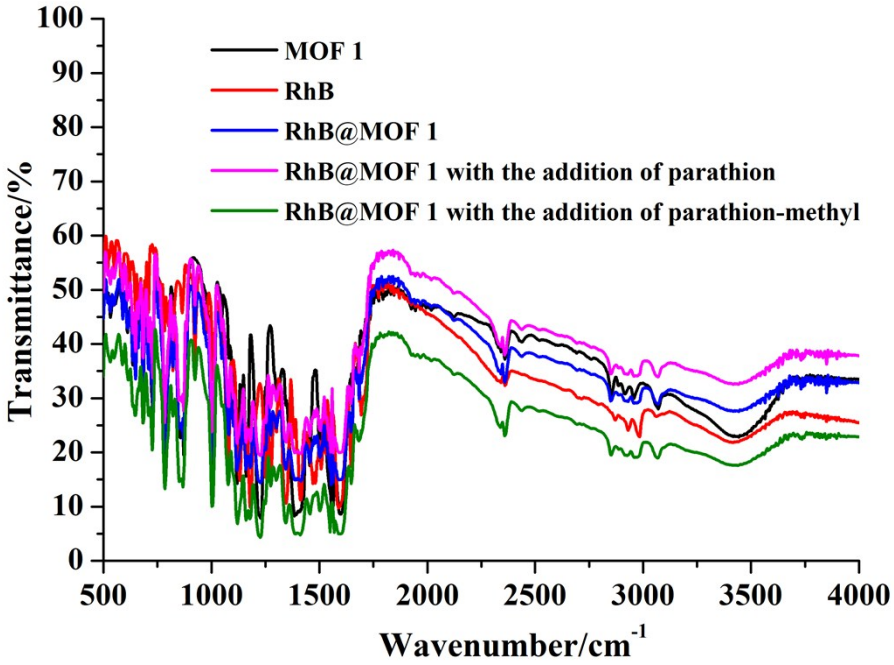

Fig. S15 The IR for RhB@LMOF **1** after the detecting experiment.

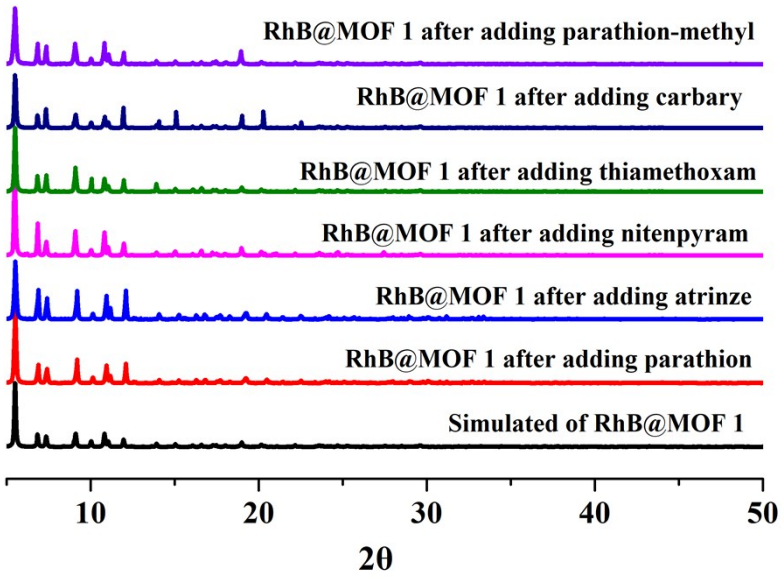

Fig. S16 The PXRD for RhB@LMOF **1** after the detecting experiment.

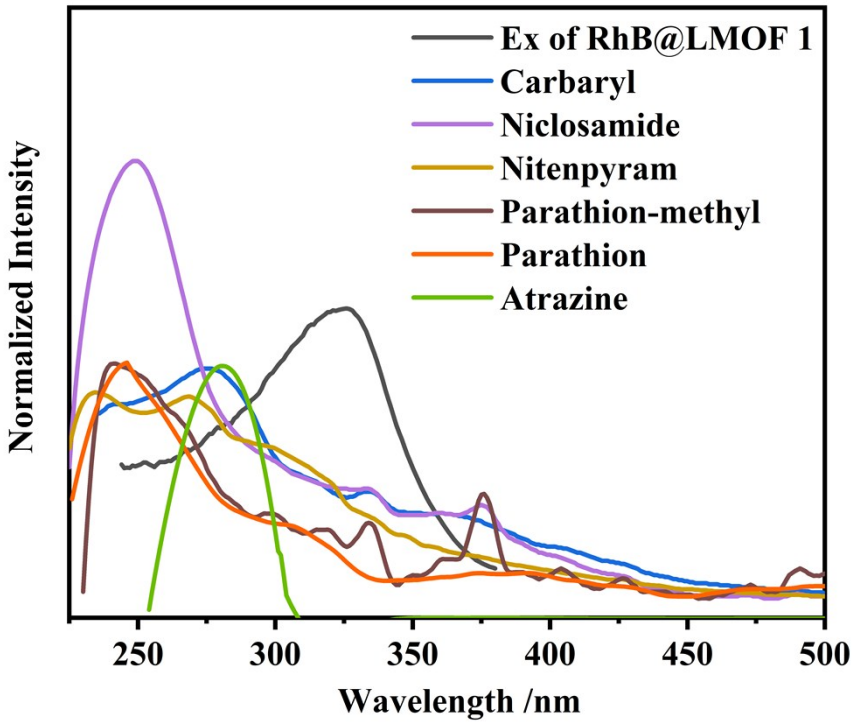

Fig. S17. The exaction spectrum of RhB@LMOF **1**.